




Synthesis and Characterization of Graphene-Based Inks for Spray-Coating Applications

D.S. SAIDINA,^{1,2} S.A. ZUBIR,¹ S. FONTANA,² C. HÉROLD,²
and M. MARIATTI ^{1,3}

1.—School of Materials and Mineral Resources Engineering, Engineering Campus, Universiti Sains Malaysia, 14300 Nibong Tebal, Pulau Pinang, Malaysia. 2.—Institut Jean Lamour, Campus Artem, 2 allée André Guinier, BP 50840, 54011 Nancy Cedex, France. 3.—e-mail: mariatti@usm.my

Conductive inks made of graphene-like materials have attracted significant attention due to their extraordinary electrical properties. In this study, three different types of graphene-like materials, namely, graphene foam (GF), graphite nanoplatelets (GNPs) and synthetic graphite (SG), are utilized to fabricate conductive inks for printable flexible electronics applications. The results show that GF exhibits the highest surface area and pore volume, while GNPs and SG display large lateral sizes, highly crystalline structures and high-quality particles. In addition, the quality of the sprayed patterns are mainly influenced by the properties of graphene-based inks. The properties of conductive inks made from various graphene-like materials, including the viscosity, contact angle and surface energy, are investigated. The viscosity and contact angle of the conductive inks increase markedly with increasing filler loadings in a polyester varnish (PV) binder. Based on the electrical conductivity of unfilled PV, the conductive ink made of GNPs exhibits a 186% improvement in electrical conductivity at 10 vol% filler loading compared to those of 40% and 10% shown by SG and GF, respectively.

Key words: Graphene, conductive inks, spray coating

INTRODUCTION

Conductive ink is one of the main elements in the printing industry, including inkjet printing, spray coating and screen printing, for flexible electronic applications. Recently, conductive ink made of graphene has become a topic of interest due to its superior electrical properties in comparison to various nanomaterials, including metals, oxide nanoparticles and other carbon-based materials. Conductive ink is one of the main components in the fabrication of flexible electronics, acting as a printed object on a flexible substrate that conducts electricity. Graphene, a novel 2D carbon nanomaterial, has provoked significant research interest recently due to its large specific surface area of $2630 \text{ m}^2 \text{ g}^{-1}$, high

electrical conductivity of up to 6000 S/cm , optical transparency of 97.7%, extraordinary electron mobility of $200,000 \text{ cm}^2 \text{ v}^{-1} \text{ s}^{-1}$, thermal conductivity of $5000 \text{ W m}^{-1} \text{ K}^{-1}$ and superior mechanical properties with an elastic modulus of 0.25 TPa and an ultimate strength of 130 GPa.^{1–3} As reported by Wallace in 1947⁴, almost all ‘graphene-like materials’ are different from the idealized 2D ‘graphene structure’. Several types of graphene-like materials exist, from monolayer to multilayer graphene, turbostratic carbon, graphite nanoplatelets (GNPs), nanosheets, nanoflakes and graphene oxide (GO).

Several methods for the mass production of graphene-like materials have been studied, such as chemical vapor deposition, liquid phase exfoliation (LPE), graphite oxide routes leading to GO or reduced graphene oxide and electrochemical routes.^{5–7} LPE is considered to be the simplest method and yields larger quantities of graphene; however, the number of graphene layers is inconsistent as the layers may

(Received February 1, 2019; accepted June 13, 2019; published online June 25, 2019)

reaggregate, and the method introduces defects in the graphene layers that may then not be suitable for use as conductive inks.⁸ Therefore, an alternative method based on a solvothermal reaction is also used in order to prepare graphene-like materials. This solvothermal method is an alternative bottom-up approach for the production of graphene and is known for its few high-quality layers of graphene, simple operation, low cost of raw materials, environmentally friendly reactants, mild synthesis conditions and ability to yield graphene on a large scale.⁹ This process enables the synthesis of materials with particular structures and properties. The solvothermal reaction method has been previously studied for the fabrication of carbon materials, and especially graphene foam (GF), also known as turbostratic carbon.^{10,11}

Many studies have considered GNPs and GO as graphene-based inks; however, there are limited studies utilizing GF produced by using the solvothermal reaction method for conductive inks. The unique structure of GF, which is constructed of a 3D interconnected network to avoid aggregation, while maintaining electrical conductivity, can be explored for the fabrication of graphene-based inks. Therefore, this study compares the performance of GF with GNPs and synthetic graphite (SG), and is divided into two parts: characterization of the graphene-like materials and the properties of graphene-based inks. The graphene-like materials are first characterized by investigating the morphology, phase formation, functionalities, structural characteristics and electrical properties. The conductive inks made of graphene-like materials mixed with polyester varnish (PV) binder are further investigated by measuring the viscosity, contact angle and surface energy values and also the electrical properties of the sprayed patterns.

MATERIALS AND METHODOLOGY

Materials

The PV (ULTIMEG 2000/380) used in this study was supplied by AEV, UK, with a density of 0.92 g/cm³, and was used as a binder. The solvent was ULTIMEG 2000 T4 Thinners supplied by AEV, with a density of 0.87 g/cm³. GF was elaborated using a solvothermal reaction method based on previous work by Speyer et al.¹¹ The density of the GF was 1.06 g/cm³. GNP and SG powders with densities of 2.23 g/cm³ and 3 g/cm³, respectively, were supplied by the Timcal Group, Switzerland, and were used as fillers for comparison. The measured electrical conductivities of the GF, GNP and SG films, as well as the PV pattern, were 1.90×10^{-10} S/cm, 0.56×10^{-10} S/cm, 0.39×10^{-10} S/cm and 7.2×10^{-10} S/cm, respectively.

Fabrication of Conductive Ink Pattern

The production of conductive ink mixed with PV binder was further divided into two parts: (1) the

preparation of graphene-based inks, and (2) the fabrication of conductive ink patterns using the spray-coating method.

Preparation of Conductive Inks

The loading of graphene-like materials in the PV binder was varied from 2 to 20 vol%. The formulations were sonicated at room temperature for 15 min with a 175-W power density in order to achieve a uniform and homogenous dispersion of the filler in the PV binder. The temperature of the mixture increased during the sonication process. Therefore, in order to avoid the mixture overheating, the beaker was immersed in a water bath to reduce the temperature. Different loadings of GF, GNPs and SG in the PV binder were used in the study due to the density difference of the fillers, which subsequently influence the viscosity of the mixture.

Fabrication of Conductive Ink Pattern Using Spray Coating Method

In order to achieve a highly uniform deposition, a customized motor-controlled air-spray coating was fabricated to deposit the mixture of conductive ink and PV onto a flexible substrate. The flexible substrate used in this study was an organic transparent film. The flexible substrate was placed on the preheated metal substrate. The metal substrate temperature, the spray length and the air pressure were fixed at 100°C, 0.16 m and 4 psi, respectively. The conductive ink pattern produced by spray coating was cured at 130°C for 4 h. The schematic of flow work for the fabrication process of conductive ink pattern, the digital image of the conductive ink pattern and scanning electron microscope (SEM) images from the top-view of the conductive ink patterns are shown in Fig. 1. From the micrographs, it can be observed that the conductive ink patterns were sprayed evenly and homogeneously throughout the substrate, and that the graphene-like materials were fully coated by the PV binder.

Characterization

The flake size and microstructure of the graphene-like materials, as well as the morphology of the conductive ink patterns, were characterized by using SEM (model QUANTA FEG450 and JEOL JSM-6010LA). The thickness, morphology and lattice arrangement of the graphitic material through selected area electron diffraction (SAED) were characterized by using high-resolution transmission electron microscopy (HRTEM; model FEI TECNAI G20). The graphene-like materials were sprinkled onto the surface of sticky carbon tape for SEM analysis. Meanwhile, for the HRTEM measurements, the graphene-like materials were dispersed in ethanol and a drop of the dispersion was deposited on a copper grid covered with a holey

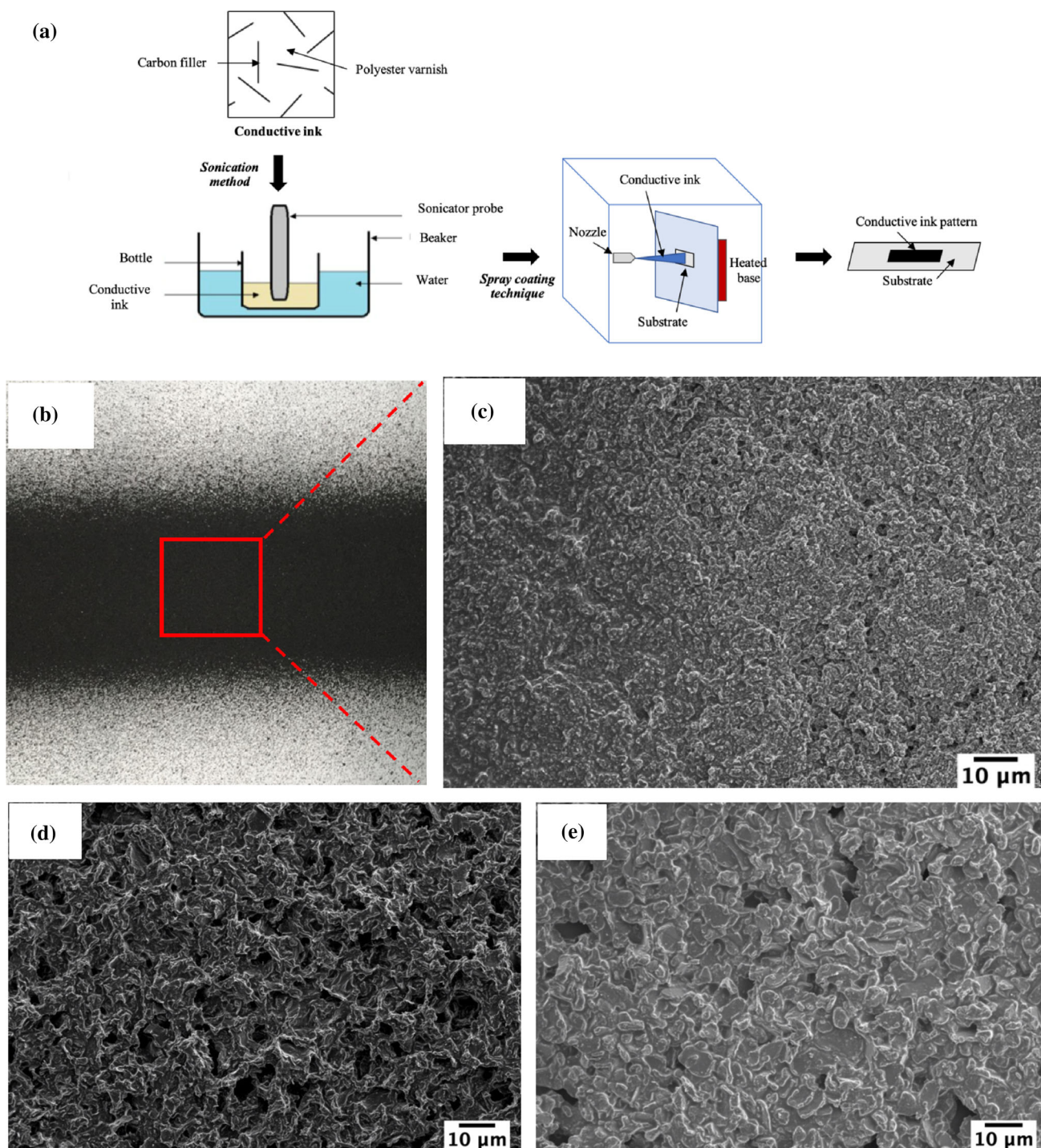


Fig. 1. (a) Schematic of the fabrication process of conductive ink pattern, (b) digital image of the sprayed ink pattern, and SEM images from top-view of (c) GF pattern, (d) GNP pattern and (e) SG pattern ($\times 100$).

carbon film, followed by solvent evaporation in the open air at room temperature. The specific surface area was calculated using the Brunauer–Emmett–Teller (BET) method and the micropore volume was determined using the 2D-NLDFT t -plot model (Micromeritics ASAP 2020). The structural characteristics of the graphene-like materials were

analyzed using Raman spectroscopy (Renishaw inVia Raman spectrometer) operating with a $\lambda = 633 \text{ nm}$ HeNe laser (20 mW) at a spectral range of $100\text{--}3200 \text{ cm}^{-1}$. The surface chemical bonds and the functionalities of the graphene-like materials were confirmed by x-ray photoelectron (XPS). The XPS spectra were obtained using an

AXID Ultra DLD, Kratos, equipped with an Al K α x-ray source (1486.6 eV).

The ink viscosity, η , was measured by a cone and plate rheometer at a shear rate within a range of 1–500 s⁻¹ and compared with the Carreau model (Physica MCR 301; Anton Paar Malaysia Sdn. Bhd.). The contact angle, θ_c , of the conductive ink was measured by the sessile drop method with a droplet volume of 5 μ L using a goniometer (Rame Hart Instrument, USA) on the transparent film. DROPimage Advanced software was used to obtain the contact angle. The electrical conductivity of the films and the conductive ink pattern were measured at room temperature using a four-point probe measurement. The sheet resistivity was calculated using Van Der Pauw's method. The samples were placed at the center of the copper plate and connected to the power source and voltmeter. This method was based on two voltage measurements, by shifting the two measuring devices. The power source was provided by a Keithley 2010 multimeter and the voltmeter was provided by a Keithley 220 current source. To obey Ohm's law, three current values for the measurements were applied at 50, 100 and 150 μ A, respectively. For PV, the electrical conductivity was measured using a Prostat PRS-812 resistance meter.

RESULTS AND DISCUSSION

Characterization of Graphene-Like Materials

Figure 2 shows the SEM images of the graphene-like materials: (a) GF; (c) GNP; (e) SG. Based on the micrographs, it can be seen that the structure for GF is a 3D porous structure. The porous GF was formed due to the reaction between ethanol and sodium during the solvothermal process. Ethanol is encapsulated into sodium in a clathrate-like structure. Meanwhile, the 2D network of GNPs and SG represents the typical sheet-like morphology with folding and crumples over the sheets. The EDX spectrum of GF (Fig. 2b) shows signals for the presence of carbon, oxygen and sodium with weight percentages of 77.62, 20.03 and 2.35, respectively. The presence of oxygen and sodium is attributed to the sodium carbonate formed upon the pyrolysis reaction. Meanwhile, for the EDX spectra of GNPs (Fig. 2d) and SG (Fig. 2f), only a carbon signal was observed with a weight percentage of 100.

The size distribution of the graphene-like materials is summarized in Fig. 2g, h, i based on the SEM image analysis of over 150 particles with more than six different locations using ImageJ software. The lateral size of GF, GNP and SG particles are distributed over a broad range with mean values of 32, 38 and 44 μ m, respectively. In addition, the BET surface area and pore volume of the particles are reported in Table I. The GF exhibited the highest surface area and pore volume compared to GNP and SG. This is attributed to the 3D porous structure, which prevents the restacking of GF particles.

Meanwhile, the GNP and SG sheets restack themselves and agglomerate due to strong van der Waals interactions and high inter-sheet junction contact resistance.¹²

Figure 3 illustrates the HRTEM images of (a, b) GF, (c, d) GNP and (e, f) SG particles. Based on Fig. 3a, it is observed that very thin areas with folded edges almost throughout the GF structure and amorphous carbon regions can be seen. The presence of amorphous carbon region is due to the crystallisation of GF, which is not completed.¹¹ Eleven parallel lines were observed from the image captured by HRTEM, an early indication that it was a multi-layer graphene. Meanwhile, the GNP and SG samples indicated transparent sheet-like structures and suggested that the graphene-like materials presented better crystallinity with ordered planar regions. The number of graphene layers for GNP and SG were 10 and 46 layers, respectively. In addition, GNPs and SG also exhibited crumpled and less folded edges compared to GF. The folded edges appeared more in the GF structure than in the GNP and SG structures, due to the tendency of GF particles to overlap as a result of the high surface area of the extended thin layers. The interlayer distances for GF, GNPs and SG were 0.33, 0.34 and 0.33 nm, respectively, in agreement with a graphitic stacking.

The crystallographic structure of the graphene-like materials was characterized by SAED, as shown in Figs. 3g, h, i. The SAED for the GF particles exhibited a diffraction ring pattern, which indicates polycrystalline features in an amorphous material. In contrast, the symmetrical and isolated points arranged in a hexagonal pattern show the high crystallinity of the GNP particles. Meanwhile, the SAED for SG with 46 layers exhibited the disorderly lattice arrangement showing how thick the particle was. Similar patterns were observed by Htwe et al.¹³ in their study on the formation of graphene using an electrochemical exfoliation process.

Figure 4 shows the Raman spectra of the graphene-like materials. Raman spectroscopy is a versatile tool for obtaining useful information about carbonaceous materials. There are three disorder-related bands that are prominent for Raman spectra of graphite, including the D peak at around 1350 cm⁻¹, the G peak at around 1580 cm⁻¹ and the 2D peak at around 2700 cm⁻¹. By using the Raman spectra, it is possible to identify the amounts of defects and their types (D band), in-plane sp² hybridized carbon atoms (G band), stacking order, and the number of layers (2D band) in graphene samples.^{14,15}

In general, similar peaks were observed in the three types of graphene-like materials. In Fig. 4 for the GF sample, the Raman spectrum showed peaks at 1329 cm⁻¹ (D band), 1589 cm⁻¹ (G band) and 2663 cm⁻¹ (2D band). For the GNP sample, the Raman sample exhibited peaks at 1339 cm⁻¹ (D

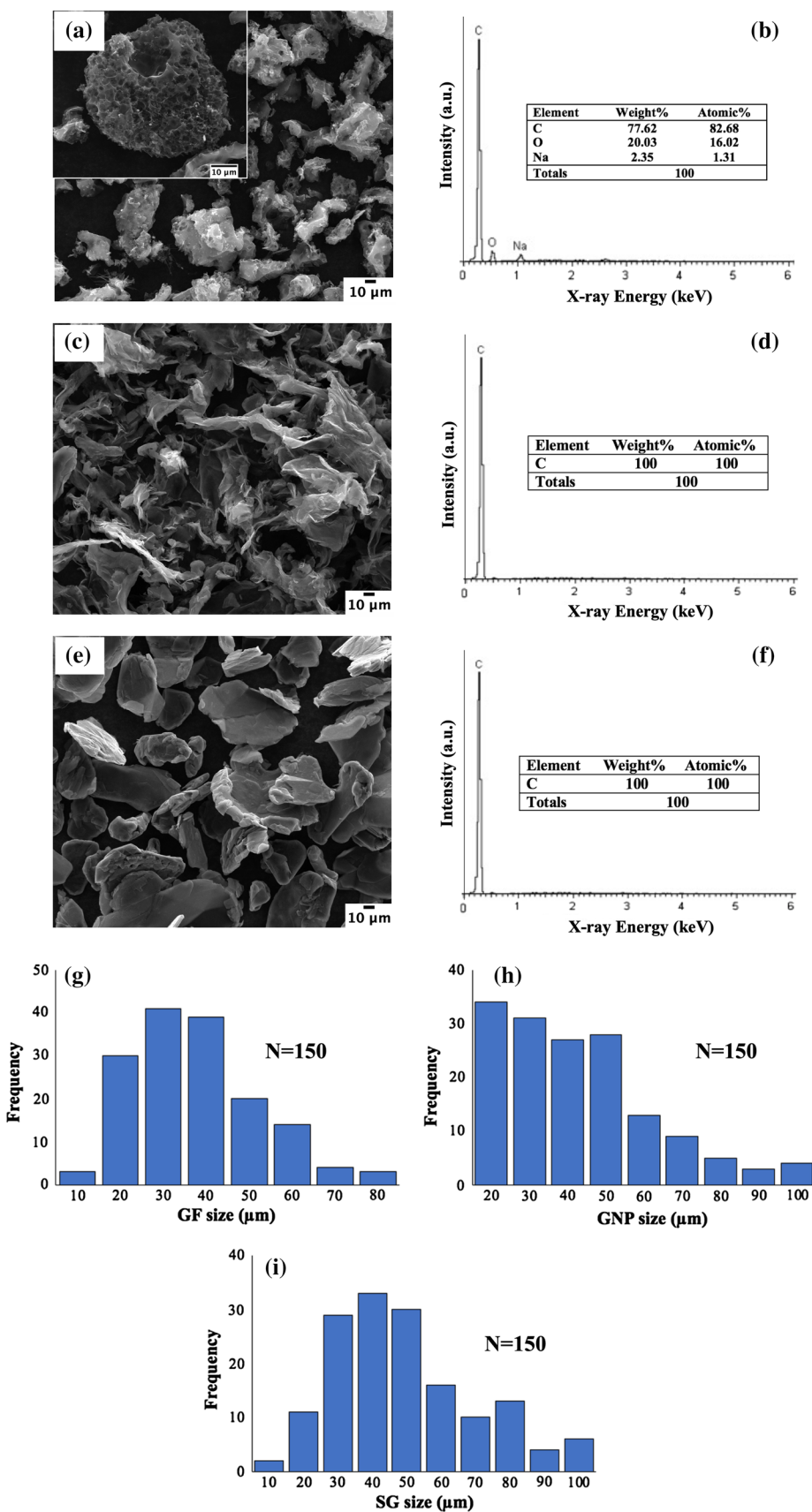


Fig. 2. SEM micrographs of (a) GF, (c) GNP and (e) SG particles ($\times 1000$), the *inset* is an image of porous GF at $\times 2000$, EDX analysis of (b) GF, (d) GNP and (f) SG and lateral size distribution histogram measured by ImageJ of (g) GF, (h) GNP and (i) SG particles.

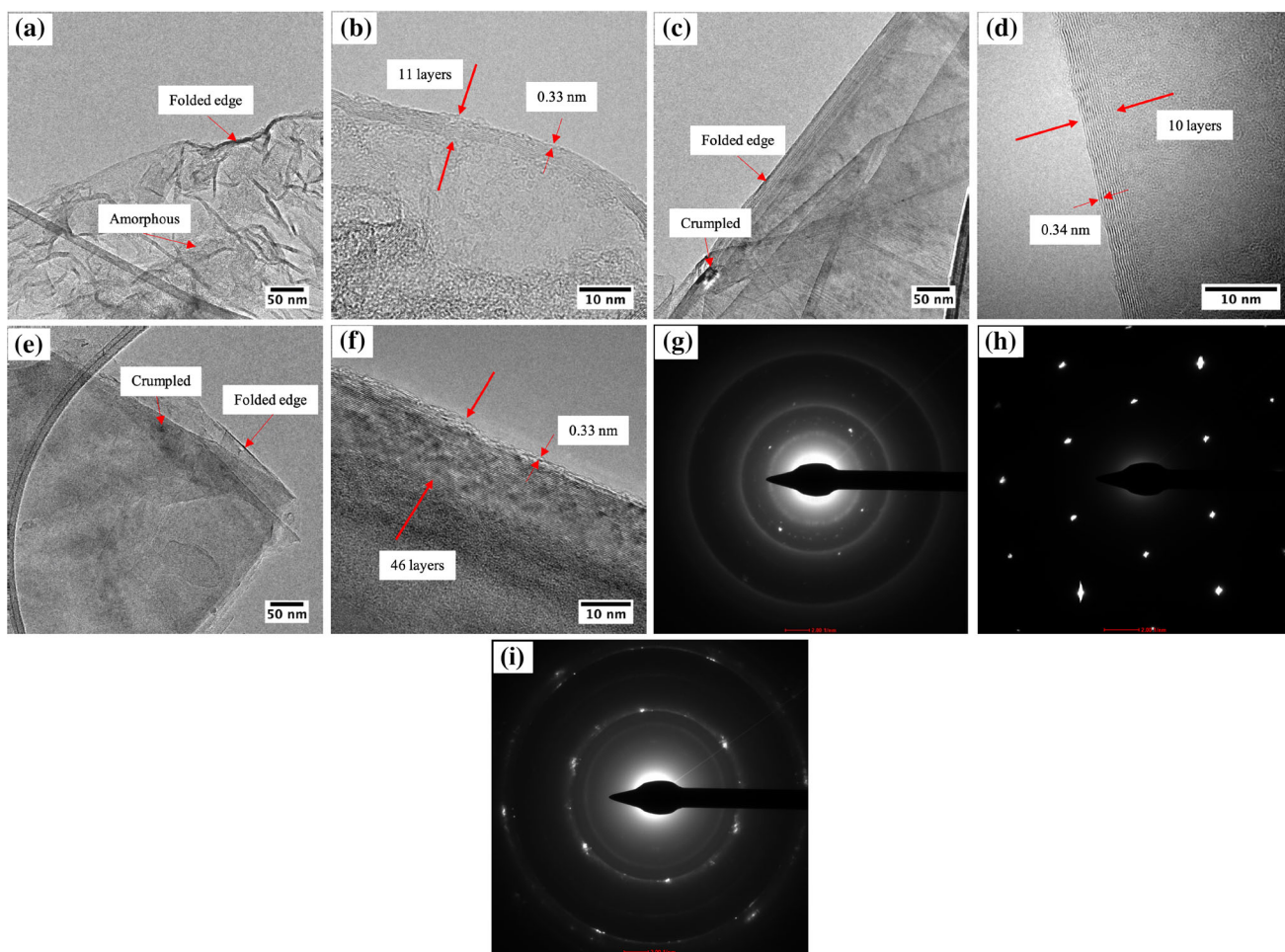


Fig. 3. HRTEM micrographs of (a, b) GF, (c, d) GNP and (e, f) SG particles at magnifications of (a, c, e) 97 kX and (b, d, f) 690 kX; SAED of (g) GF, (h) GNP and (i) SG particles.

Table I. BET surface area and pore volume of the graphene-like materials

Sample	BET surface area ($\text{m}^2 \text{g}^{-1}$)	Pore volume ($\text{cm}^3 \text{g}^{-1}$)
GF	2136	0.138
GNP	25	0.003
SG	3	0.001

band), 1581 cm^{-1} (G band) and 2689 cm^{-1} (2D band). Meanwhile, for the SG sample, the Raman spectrum presented peaks at 1346 cm^{-1} (D band), 1580 cm^{-1} (G band) and 2685 cm^{-1} (2D band). The broadening of the D and G bands of the GF spectrum is attributed to the presence of amorphous carbon.¹⁶ Furthermore, two additional peaks were observed for the GF spectrum at $\sim 1150 \text{ cm}^{-1}$ (A band), corresponding to nanocrystalline diamond and sp^3 defects, and also at $\sim 1450 \text{ cm}^{-1}$ (B band), corresponding to nanocrystalline graphite and sp^2 clusters in a sp^3 matrix.^{16–18} The additional peaks observed for the GF spectrum are consistent with

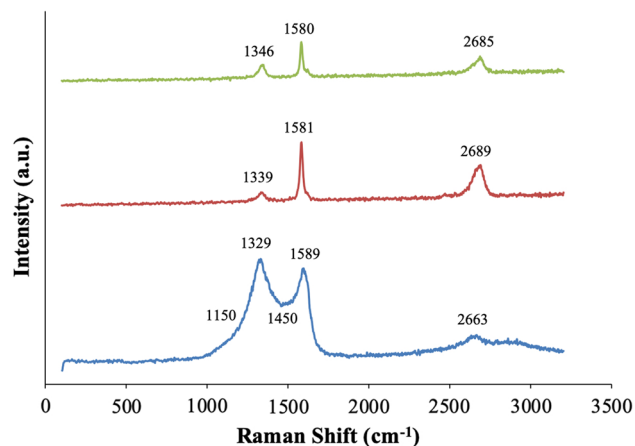


Fig. 4. Raman spectra of (a) GF, (b) GNP and (c) SG particles.

previous work by Speyer et al.¹⁶ confirming the presence of A and B bands.

The defects of the particles can be determined by measuring the intensity ratio of the D and G peaks (I_D/I_G).¹⁹ Based on Table II, the intensity ratios of

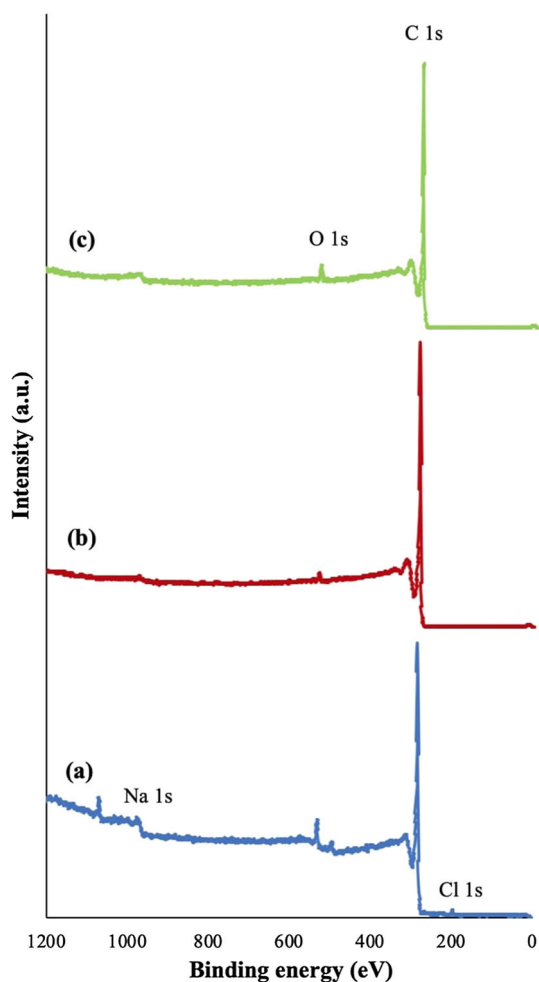


Fig. 5. XPS spectra of (a) GF, (b) GNP and (c) SG particles.

the D band to the G band (I_D/I_G) of GF, GNPs and SG were calculated as 1.07, 0.34 and 0.56, respectively. The higher value of I_D/I_G can be related to the higher degree of disorder or higher defect concentration. From the result, the GF sample exhibited the highest value of I_D/I_G compared to those of the GNP and SG samples, meaning that the large area of GF has low structural quality. In addition, for AB-stacked graphene, the number of layers can be derived from the ratio of peak intensities for 2D and G (I_{2D}/I_G). The ratios of I_{2D}/I_G for GF, GNPs and SG were 0.42, 0.70 and 0.74, respectively, indicating that the graphene-like materials consist of multi-layer graphene.

The surface characterization, chemical composition, types of carbon and oxygen bonds, and the percentage of oxygen present in the graphene-like materials were investigated using XPS, as illustrated in Fig. 5a–c. The XPS spectra are dominated by features at 284 and 532 eV, corresponding to C 1s and O 1s, respectively. The peak corresponding to C 1s suggests that sp^2 hybridized carbon atoms exist in the graphene-like materials, while the peak related to O 1s indicates the presence of various

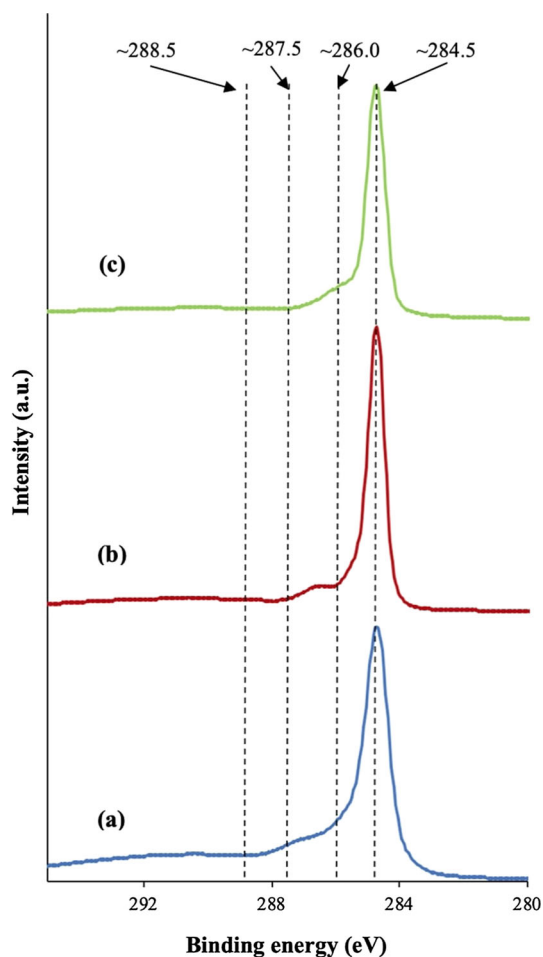


Fig. 6. C 1s spectra bands of (a) GF, (b) GNP and (c) SG particles.

Table II. Raman intensity of the graphene-like materials

Sample	I_D	I_G	I_{2D}	I_D/I_G	I_{2D}/I_G
GF	1511	1400	594	1.07	0.42
GNP	312	918	642	0.34	0.70
SG	351	622	458	0.56	0.74

oxygen functionalizations in the graphene-like materials structure.^{13,20,21} For the GF particles, chloride and sodium were detected as contaminants, as a result of sodium carbonate being trapped in carbon structures even after washing with concentrated hydrochloric acid. The carbon, oxygen and the O/C ratio were obtained through elemental analysis measurements by XPS analysis, as presented in Table III. The graphene-like materials showed approximately 0.050, 0.008 and 0.017 carbon to oxygen weight ratios for the GF, GNP and SG particles, respectively. The higher oxygen content in the GF particles is attributed to the sodium carbonate formed during the pyrolysis reaction, parallel with the SEM–EDX results.

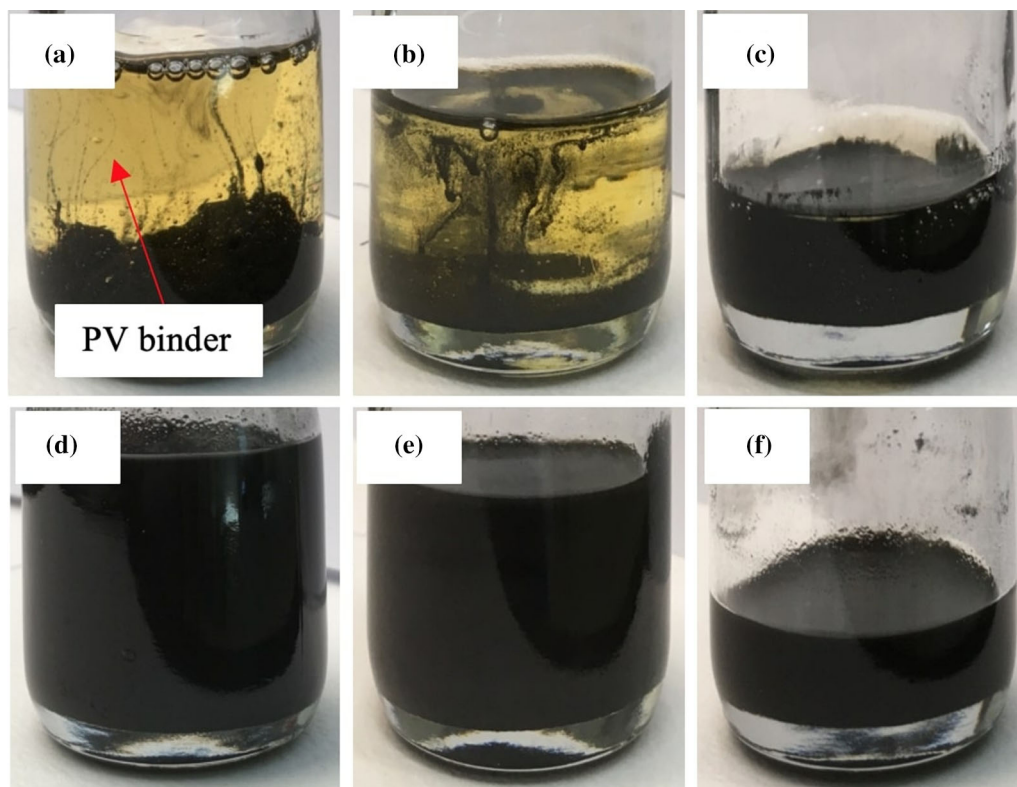


Fig. 7. Digital images of (a, d) GNP ink, (b, e) SG ink and (c, f) GF ink were observed at (a–c) before sonication and (d–f) after sonication (day 1).

The peak at ~ 284 eV was deconvoluted in order to understand the oxygen functionality in the graphene-like materials. Further deconvolution of the C 1s peak, as presented in Fig. 6, shows that the majority of the binding energy comes from sp^2 C=C, C–O, C=O and O–C=O bonds. The main peak at a binding energy of 284.5 eV is assigned to the C=C bond representing sp^2 hybridized carbon atoms in the graphene-like materials sheet. The three peaks at 286.0, 287.5 and 288.5 eV correspond to C–O (epoxide), C=O (carbonyl) and O–C=O (carboxyl COOH), respectively. This observation is in accordance with the previous work by Johra et al., where the C 1s spectrum of graphene contains four peaks at 284.6, 286.6, 287.5 and 288.5 eV.²² The multi-layer GNP has a reasonable quality, followed by SG and GF, in agreement with the Raman results.

Properties of Graphene-Based Inks

The graphene-like materials mixed with PV binder were observed over time, before and after 15 min of sonication time, as presented in Fig. 7. As can be observed, all graphene-like materials dispersed well with PV after sonication, which turned from a yellowish solution to a black solution.

Figure 8a illustrates the viscosity, η , curves of graphene-based inks at 5 vol% as a function of shear rate. It was observed that the η for all inks

decreased with increasing shear rate within a range of $1\text{--}500\text{ s}^{-1}$, exhibiting shear-thinning flow behavior. The η is considered to be stable at high shear rate values. The attraction between the graphene-like materials induces flocculation in the inks, which causes an immobility of the solvent suspending the particles and therefore increasing the η at low shear rates.²³ In comparison, at higher shear rates, the flocculation breaks down and promotes the mobility of solvent entrapment between particles, causing the η to be decreased.

Meanwhile, Fig. 8b shows the η variation as a function of filler loadings at a shear rate of 500 s^{-1} . It is clearly indicated that the addition of graphene-like materials at 5 vol% showed an increment in η of the inks by 505% (GNP ink), 58% (SG ink) and 19% (GF ink) compared to the unfilled PV binder. The η values of the inks were different even at the same filler loading due to the shape, size and density of the fillers. According to Timofeeva et al.,²⁴ elongated particles, such as platelets and cylinders, result in high viscosity compared to those of a spherical shape. As the porosity reduced the resistance of fluid to flow during contact with the surface, the viscosity was also reduced.^{25,26} On this basis, it can be concluded that the result was acceptable, as the viscosity for GF with a porous structure was lower than those of GNP and SG with a platelet shape.

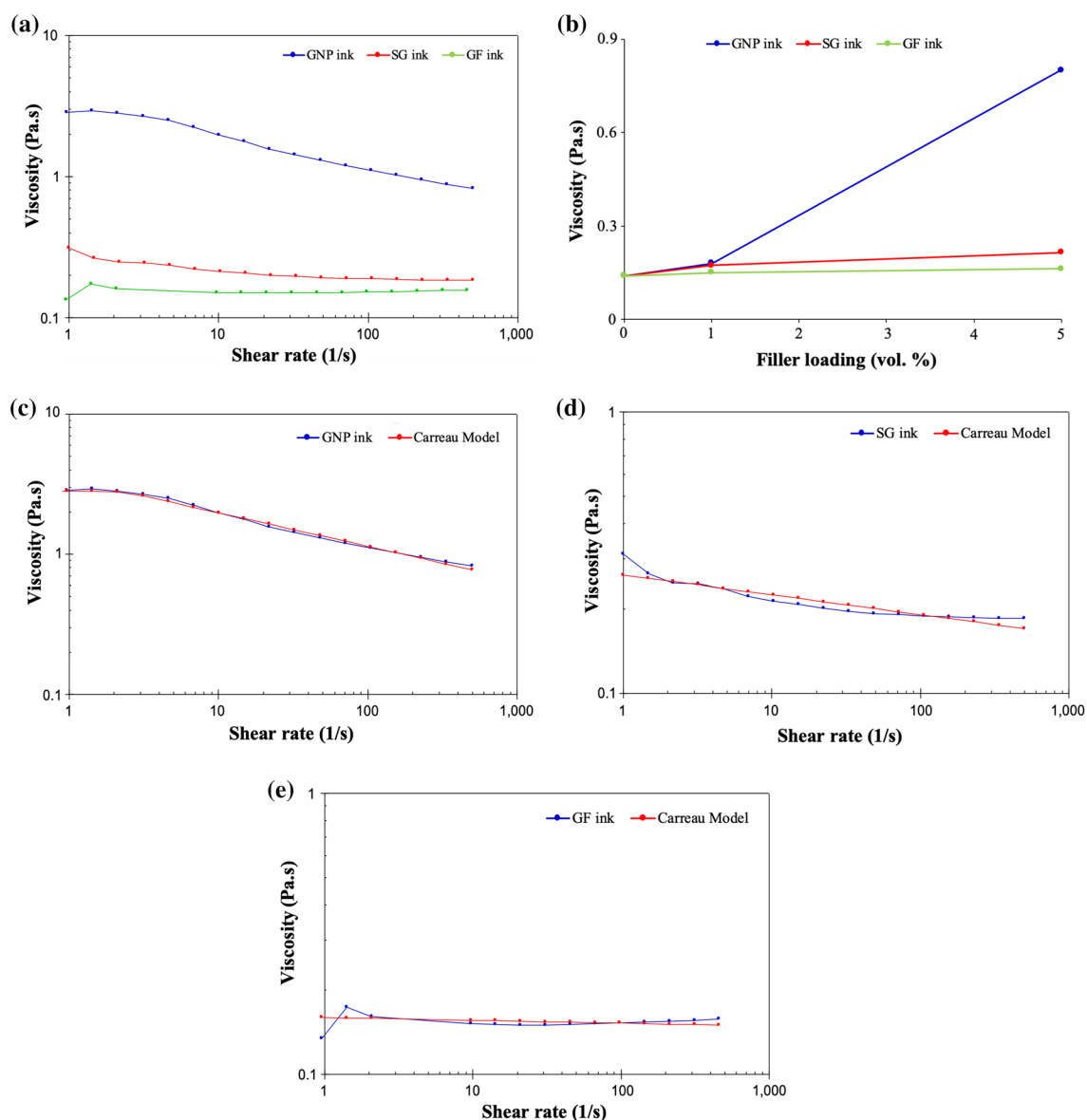


Fig. 8. (a) Viscosity curves of conductive inks at 5 vol% as a function of shear rate, (b) viscosity variation as a function of filler loading at shear rate of 500 s^{-1} , and viscosity curves of (c, f) GNP ink, (d) SG ink and (e) GF ink with a fitted Carreau Model curve at 5 vol% of filler loading.

Figure 8c–e shows the η curves as a function of shear rate predicted by the Carreau model, as well as the experimental data. The Carreau model was used to describe the behavior of fluids exhibiting shear thinning behaviour. The liquid acts as a Newtonian fluid at a low shear range and the high thinning properties are determined by the power law rule.²⁷ The equation of the Carreau model is as follows:

$$\eta(\dot{\gamma}) = \eta_{\infty} + (\eta_0 - \eta_{\infty}) \left(1 + (\lambda \dot{\gamma})^2 \right)^{\frac{n-1}{2}}$$

where η_{∞} is the viscosity at infinite shear rate, η_0 the viscosity at zero shear rate, λ the relaxation time

and n the power index. From Fig. 8c–e, the Carreau model agrees relatively well with the experimental data over a wide range of the shear rate for GNP ink, while the fits of the curves predicted for the SG and GF ink samples are less accurate, especially at low shear rates.

Besides the physical properties of the prepared inks, the surface wettability of the ink with the substrate is also a factor that influences the spray pattern quality. The contact angle, θ_c , is an indication of the wetting performance of liquids applied to solids. The contact angle is measured as the angle between the base and the tangent at the point of contact between the conductive ink and surface of the transparent film. Figure 9a, b illustrates the droplet shape just before it lands on the

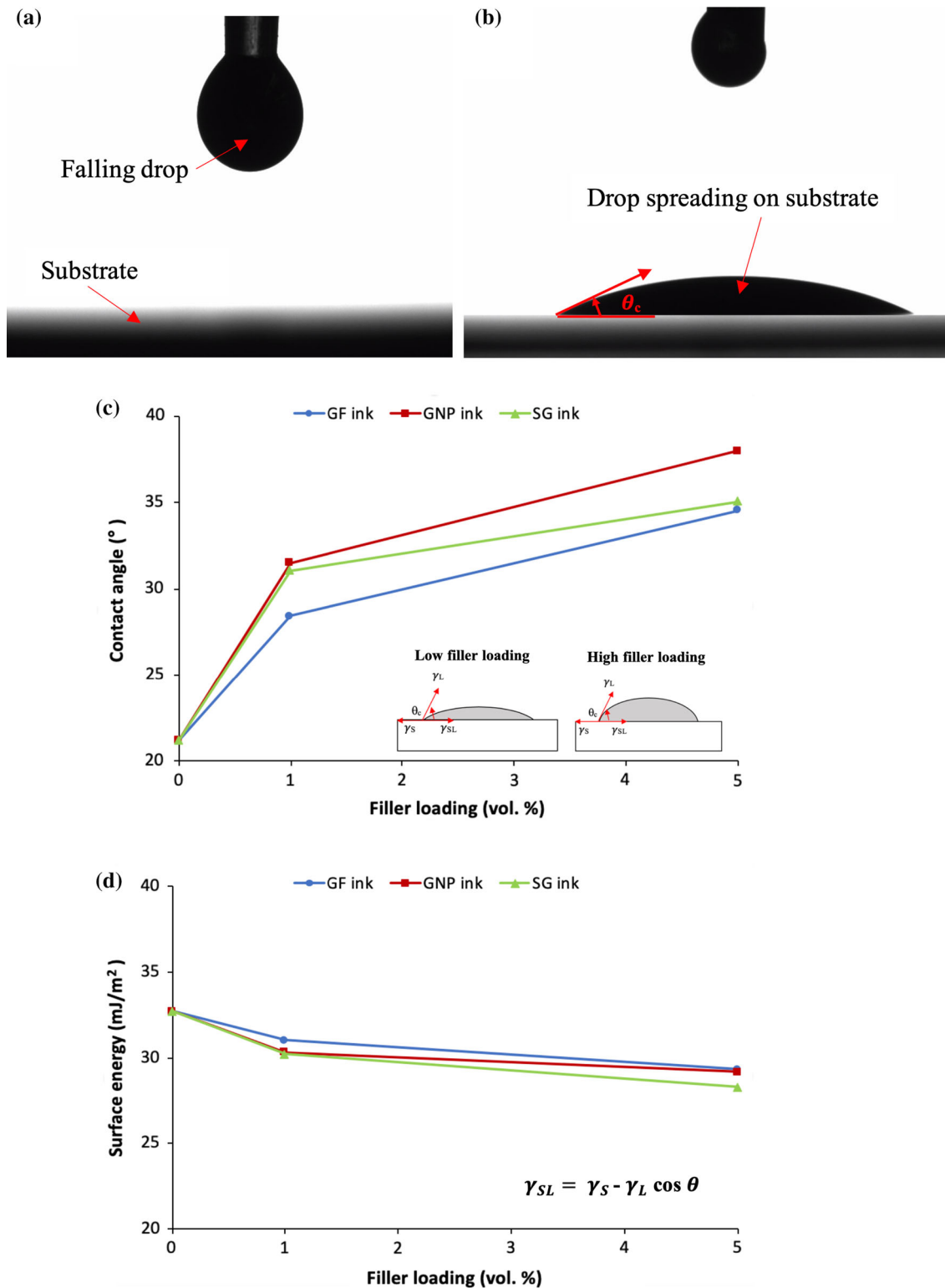


Fig. 9. Contact angle measurement (example: 1 vol% GF ink) when (a) drop falling and (b) as the drop settles on the surface of the substrate, (c) contact angle variation as a function of filler loadings; *inset* a small and a high contact angle, (d) surface energy as a function filler loadings including Young's equation.

transparency substrate and when the drop settles on the substrate. Figure 9c indicates that the θ_c for all conductive inks increased with increasing filler

loading in the PV binder. The increment in θ_c is due to the lower surface energy and the hydrophobic nature of graphene.²⁸ Nevertheless, the conductive

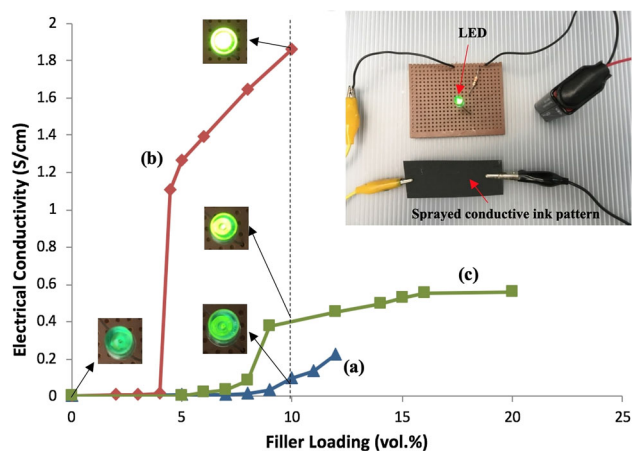


Fig. 10. Electrical conductivity of (a) GF ink, (b) GNP ink and (c) SG ink as a function of filler loading; inset digital images of an electronic circuit set up and LED brightness for conductive ink patterns at 10 vol%.

Table III. The elemental compositions of carbon (C 1s), oxygen (O 1s) and O/C atomic ratio of the graphene-like materials

Sample	C (wt%)	O (wt%)	O/C
GF	93.98	4.64	0.050
GNP	99.17	0.83	0.008
SG	98.31	1.69	0.017

inks still show hydrophilic characteristics, $\theta_c < 90^\circ$, which lead to a better ink–substrate combination.

Surface energy studies determine the intermolecular interactions at the interfaces of a solid surface with its environment. The surface energy relationship between liquid, solid and gas interfaces can be expressed by Young's equation $\gamma_S = \gamma_{SL} + \gamma_L \cos \theta$, where γ_L is the surface energy of the liquid, γ_{SL} is the surface energy between the solid to liquid interface and γ_S is the surface energy of the solid.²⁹ The γ_{SL} values from the measured θ_c for all conductive inks were calculated and are shown in Fig. 9d. The γ_{SL} is found to be at a maximum in unfilled PV (32.7 mJ/m²) and the γ_{SL} showed a slight decrease with increasing graphene-like material loading. According to the concept of the wetting process, the hydrophobic nature is observed when the solid–vapor interfacial energy is low and the tendency for spreading to eliminate the interface will be less. In order to reduce the surface energy of the system, graphene-like materials should properly interact with the PV binder. The decrement in γ_{SL} of the conductive ink with increasing graphene-like materials is an indication of the tendency of conductive inks to become less reactive with the surrounding compared to the unfilled PV. As the γ_{SL} of the conductive ink becomes lower, the polymer chains preferentially interact with the

graphene-like material surface and therefore decrease the interaction with the surroundings.³⁰

The conductive ink patterns made of various graphene-like materials at different loadings in the PV binder were fabricated in order to determine the percolation threshold. Figure 10 presents the electrical conductivity of various conductive inks as a function of filler loading. Obvious different filler loadings were used in the formulation of conductive inks based on GF, GNPs and SG due to the η . Based on the formulations, a higher amount of GF filler was used to mix with polyester varnish as compared to GNPs and SG at the same filler loading due to the low density of GF. However, the conductive inks become very difficult to dispense at higher filler loading due to high η .

It can be observed that the electrical conductivity of all the samples increased markedly with increasing filler loadings (Fig. 10). The conductive ink made of GNPs shows the highest electrical conductivity, followed by the SG and GF inks at all filler loadings. Even though the GF exhibited a higher BET surface area than those of GNPs and SG, which will increase the electrical conductivity of the conductive ink pattern, there were also other factors that influenced the electrical conductivity of GF ink, including the lateral size, crystallinity, oxygen content and quality of GF particles, as shown by BET, SEM–EDX, HRTEM, XPS and Raman analysis. Due to the above factors, the electrons in GF could not move rapidly through the interconnected network of low-quality GF. Meanwhile, the higher electrical conductivity at all filler loadings of GNP ink and SG ink were attributed to the large lateral size, high crystalline structure and high quality of GNP and SG flakes.

For the GNP ink, the percolation threshold is obtained between 4 and 4.5 vol% GNPs. On further increasing the GNP loading, the electrical conductivity is observed to be increased with values of 1.26 S/cm at 5 vol% to 1.86 S/cm at 10 vol%. For the SG and GF inks, the percolation threshold could be observed when the SG loading is inbetween 8 and 9 vol% and when the GF loading is inbetween 9 and 10 vol%.

A simple electronic circuit was composed of a 9-V battery, the sprayed conductive pattern, a capacitor and the LED to demonstrate the behavior of conductive ink patterns towards the LED brightness. An inset shows digital images of an electronic circuit set-up and LED brightness for various types of conductive ink patterns at 10 vol%. The LED connected to GNP ink pattern showed the brightest followed by SG ink pattern and GF ink pattern. GNP ink exhibited remarkable improvement of electrical conductivity, followed by SG ink and GF ink at 10 vol% than unfilled polyester varnish binder by 186, 40 and 10%, respectively.

The electrical conductivity of the conductive ink patterns is strongly dependent on their morphology, which was investigated by SEM analysis.

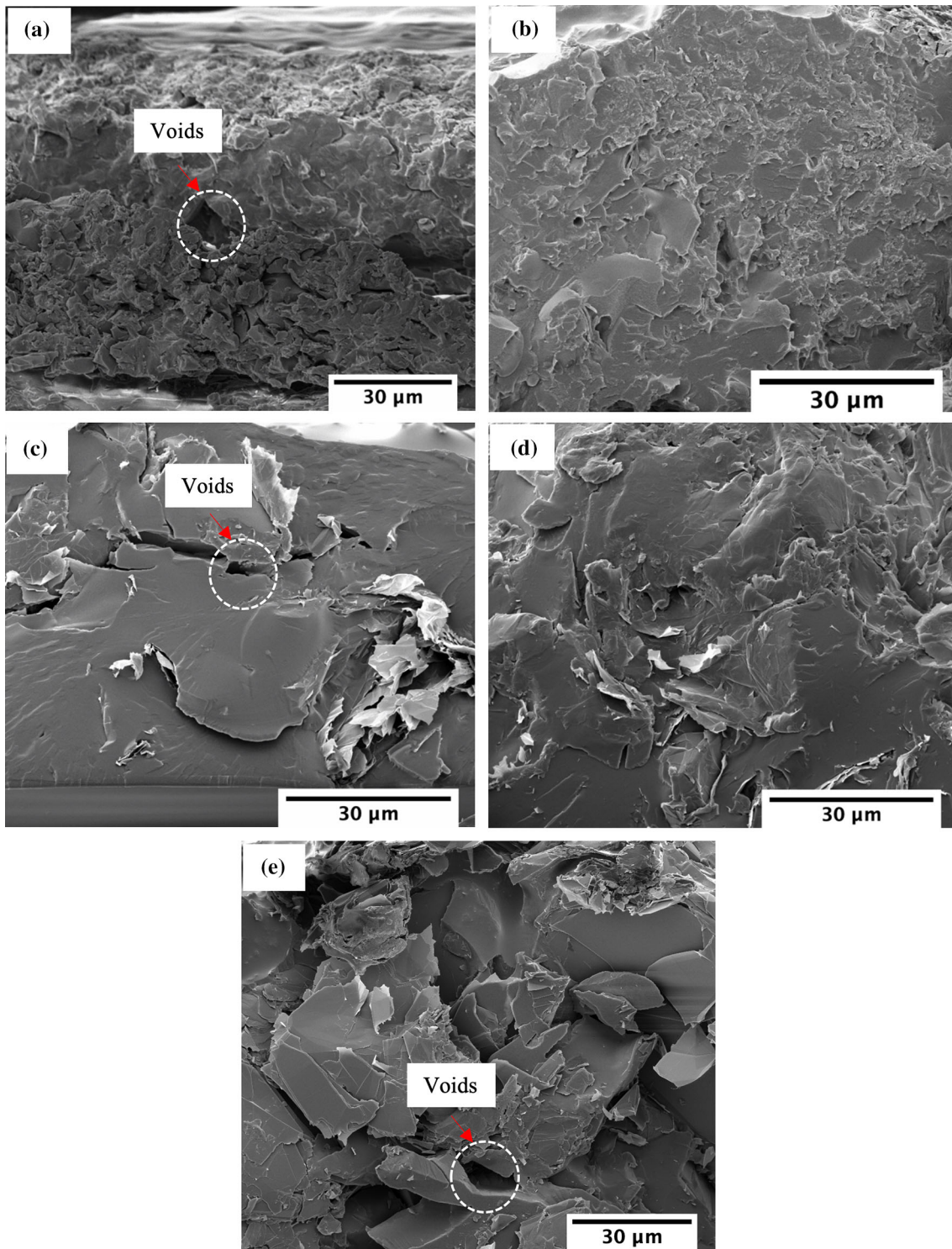


Fig. 11. SEM micrographs of cross-section conductive ink patterns made of (a) 7 vol% GF (b) 12 vol% GF, (c) 2 vol% GNP (d) 4.5 vol% GNP (e) 9 vol% SG ($\times 2500$ – 3500).

Figure 11a–e shows the morphology of the cross-section conductive ink patterns with respect to the filler loadings, which provides insight into the process of conductive network formation. The conductive ink patterns at low filler loadings (as in

Fig. 11a, c), indicating that some conductive paths were not connected and that low filler loadings were not sufficient to support a complete network and more voids could be seen. However, when the amount of graphene-like materials were increased,

Table IV. Comparison of the maximum electrical conductivity and percolation threshold between present study and graphene-filled polymer from literature

Filler	Binder/matrix	Percolation start (vol%)	Percolation end (vol%)	Electrical conductivity at end point of percolation (S/cm)	Method of mixing and fabrication	References
Reduced graphene oxide	Ultrahigh molecular weight polyethylene	0.028	0.4	0.1	Sonication, stirring and compression molding	31
Thermally reduced graphene oxide	Polyamide-6	0.11	1.8	10^{-2}	Sonication, stirring and compression molding	32
Graphene	Polyacrylic acid hydrogel	0.4	1.25	10^{-6}	Free radical polymerization	33
Graphene nanosheets	Syndiotactic polystyrene	0.46	2.5	0.82	Solution blending and melt quench	34
Graphene nanosheets	Syndiotactic polystyrene	0.24	0.73	0.8	Sonication and filtration	35
Chemically exfoliated graphene	Poly(methyl methacrylate)	0.29	5.67	1.58	Internal mixing and compression molding	36
Graphene nanoplatelets	Polypropylene	2.99	9.3	1.7×10^{-2}	Mechanically mixing and injection molding	37
Graphene nanoplatelets	Polyester varnish	4.5	10	1.86	Sonication and spray coating	Present work
Synthetic graphite	Polyester varnish	9	20	0.4	Sonication and spray coating	Present work
Graphene foam	Polyester varnish	10	12	0.22	Sonication and spray coating	Present work

as shown in Fig. 11b, d, e, the network became obviously denser and the conductive pathways were well established.

Table IV compares the values of maximum electrical conductivity and corresponding percolation threshold measured in the current study with those reported in the literature for graphene filled or mixed with polymer. The present GNP ink-based conductive ink exhibited a maximum conductivity of 1.86 S/cm, which is significantly higher than the typical 10^{-6} to 1.58 S/cm values observed in the literature.^{31–37} Meanwhile, the SG and GF inks showed moderate values of maximum conductivity that remain interesting in spite of the high amount of filler loading.

CONCLUSIONS

GF was synthesized using a solvothermal reaction method and the properties were compared with commercialized GNPs and SG. GF exhibited the highest BET surface area and pore volume compared to GNP and SG. However, GF particles with small lateral size, low crystalline structure and high oxygen content reduced the electrical properties. Graphene-like materials were mixed with a PV binder to produce graphene-based inks and the properties were investigated. In general, addition of filler loadings increased the viscosity and contact angle of the conductive inks. GNP ink exhibited the highest electrical conductivity, followed by SG ink and GF ink. The micrographs of graphene-like materials in the PV binder showed that the conductive inks were evenly sprayed on the substrate. The results indicated that the ink properties used in spray coating affect the quality of a produced pattern.

ACKNOWLEDGMENTS

The authors acknowledge the financial support from the Ministry of Education Malaysia through the Fundamental Research Grant Scheme (FRGS MRSA; Grant No. 6071385). The authors also gratefully acknowledge the support from Universiti Sains Malaysia, the School of Materials and Mineral Resources Engineering. We were also grateful to Carbon Materials Group (E205)'s laboratory, Institut Jean Lamour, Université de Lorraine, France, as well as Campus France for the support.

REFERENCES

1. V. Singh, D. Joung, L. Zhai, S. Das, S.I. Khondaker, and S. Seal, *Prog. Mater. Sci.* 56, 1178 (2011).
2. K.S. Novoselov, D. Jiang, F. Schedin, T.J. Booth, V.V. Khotkevich, S.V. Morozov, and A.K. Geim, *Proc. Natl. Acad. Sci. U.S.A.* 102, 10451 (2005).
3. N.A.A. Ghany, S.A. Elsherif, and H.T. Handal, *Surf. Interfaces* 9, 93 (2017).
4. P.R. Wallace, *Phys. Rev.* 71, 622 (1947).
5. G. Chen, W. Weng, D. Wu, C. Wu, J. Lu, P. Wang, and X. Chen, *Carbon* 42, 753 (2004).

6. D. Deng, S. Feng, M. Shi, and C. Huang, *J. Mater. Sci.: Mater. Electron.* 28, 15411 (2017).
7. C.T.J. Low, F.C. Walsh, M.H. Chakrabarti, M.A. Hashim, and M.A. Hussain, *Carbon* 54, 1 (2013).
8. A. Bagri, C. Mattevi, M. Acik, Y.J. Chabal, M. Chhowalla, and V.B. Shenoy, *Nat. Chem.* 2, 581 (2010).
9. M. Choucair, P. Thordarson, and J.A. Stride, *Nat. Nanotechnol.* 4, 30 (2009).
10. G. Hu, D. Ma, M. Cheng, L. Liu, and X. Bao, *Chem. Commun.* 17, 1948 (2002).
11. L. Speyer, S. Fontana, S. Cahen, J. Ghanbaja, G. Medjahdi, and C. Hérold, *Solid State Sci.* 50, 42 (2015).
12. O. Bagri, M. Rahman, H. Younes, S. Shah, and A. Al-Ghaferi, *J. Nanomed. Nanotechnol.* 8, 1 (2017).
13. Y.Z.N. Htwe, W.S. Chow, Y. Suda, A.A. Thant, and M. Mariatti, *Appl. Surf. Sci.* 469, 951 (2019).
14. A.C. Ferrari, J.C. Meyer, V. Scardaci, C. Casiraghi, M. Lazzeri, F. Mauri, S. Piscanec, D. Jiang, K.S. Novoselov, S. Roth, and A.K. Geim, *Phys. Rev. Lett.* 9, 187401 (2006).
15. L.G. Cançado, K. Takai, T. Enoki, M. Endo, Y.A. Kim, H. Misuzaki, N.L. Speziali, A. Jorio, and M.A. Pimenta, *Carbon* 46, 272 (2008).
16. L. Speyer, S. Fontana, S. Cahen, and C. Hérold, *Mater. Chem. Phys.* 219, 57 (2018).
17. A.C. Ferrari and J. Robertson, *Phys. Rev. B* 61, 14095 (2000).
18. A.C. Ferrari and J. Robertson, *Phys. Rev. B* 63, 2 (2001).
19. Z. Tang, L. Zhang, C. Zeng, T. Lin, and B. Guo, *Soft Matter* 8, 9214 (2012).
20. S.K. Sahoo and A. Mallik, *J. Mater. Chem. C* 3, 10870 (2015).
21. D. Yang, A. Velamakanni, G.L. Bozoklu, S. Park, M. Stoller, R.D. Piner, S. Stankovich, I. Jung, D.A. Field, C.A. Ventrone Jr, and R.S. Ruoff, *Carbon* 47, 145 (2009).
22. F.T. Johra, J.W. Lee, and W.G. Jung, *J. Ind. Eng. Chem.* 20, 2883 (2014).
23. K. Woo, D. Jang, Y. Kim, and J. Moon, *Ceram. Int.* 39, 7015 (2013).
24. E.V. Timofeeva, W. Yu, D.M. France, D. Singh, and J.L. Routbort, *Nanoscale Res. Lett.* 6, 182 (2011).
25. R.E. Larson and J.J.L. Higdon, *J. Fluid Mech.* 166, 449 (1986).
26. L. Hendraningrat, B. Engeset, S. Suwarno, S. Li, O. Torsæter, Paper SCA2013 062 (2013).
27. L. Dybowska-Sarapuk, K. Kielbasinski, A. Arazna, K. Futera, A. Skalski, D. Janczak, M. Sloma, and M. Jakubowska, *Nanomaterials* 8, 602 (2018).
28. D. Parobek and H. Liu, *2D Mater.* 2, 032001 (2015).
29. M. Michel, J.A. Desai, C. Biswas, and A.B. Kaul, *Nanotechnology* 27, 485602 (2016).
30. A.K. Haghi, K.M. Pravee, and S. Thomas, *Engineered Carbon Nanotubes and Nanofibrous Materials* (Cambridge: Academic Press Inc., 2018).
31. H. Hu, G. Zhang, L. Xiao, H. Wang, Q. Zhang, and Z. Zhao, *Carbon* 50, 4596 (2012).
32. M. Ma, Z. Zhu, B. Wu, S. Chen, Y. Shi, and X. Wang, *Mater. Lett.* 190, 71 (2017).
33. A. Alam, Q. Meng, G. Shi, S. Arabi, J. Ma, N. Zhao, and H.C. Kuan, *Compos. Sci. Technol.* 127, 119 (2016).
34. C. Wang, Y.C. Chiu, and C.L. Huang, *Mater. Chem. Phys.* 164, 206 (2015).
35. Y.C. Chiu, C.L. Huang, and C. Wang, *Compos. Sci. Technol.* 134, 153 (2016).
36. P. Wang, H. Chong, J. Zhang, Y. Yang, and H. Lu, *Compos. Sci. Technol.* 158, 147 (2018).
37. Y.S. Jun, J.G. Um, G. Jiang, G. Lui, and A. Yu, *Compos. Part B* 133, 218 (2018).

Publisher's Note Springer Nature remains neutral with regard to jurisdictional claims in published maps and institutional affiliations.